RGNZ/MGPB

Multispectral Remote Sensing to Delineate the Distribution Area of Scandium-Bearing Minerals in Bauxite Mining Sites, West Kalimantan Province, Indonesia

Rudarsko-geološko-naftni zbornik
(The Mining-Geology-Petroleum Engineering Bulletin)
UDC: 528.8; 622.3
DOI: 10.17794/rgn.2023.1.2

Original scientific paper

Rosmalia Dita Nugraheni[1*]; Widya Anggraini[2]; Naily S. Setiawan[3]; Cahyaningratri P. Riyandhani[4]; Dewi Syavitri[5]; Dedi Sunjaya[6]; Agustinus Nopi[7]; I Gde Sukadana[8]

[1] *Geological Engineering Dept., Faculty of Earth and Energy Technology, Universitas Trisakti, Grogol, Petamburan, Jakarta Barat, 11450, Indonesia, ORCID https://orcid.org/0000-0002-2234-6307*

[2] *PT Paramitha Persada Tama, Watu-watu, Kendari Barat, Kota Kendari, Indonesia, ORCID https://orcid.org/0000-0001-9166-6438*

[3] *Geological Engineering Dept., Faculty of Earth and Energy Technology, Universitas Trisakti, Grogol, Petamburan, Jakarta Barat, 11450, Indonesia*

[4] *Geological Engineering Dept., Faculty of Earth and Energy Technology, Universitas Trisakti, Grogol, Petamburan, Jakarta Barat, 11450, Indonesia*

[5] *Geological Engineering Dept., Faculty of Earth and Energy Technology, Universitas Trisakti, Grogol, Petamburan, Jakarta Barat, 11450, Indonesia, ORCID https://orcid.org/0000-0002-8655-2804*

[6] *Geomin Unit, PT ANTAM Tbk., Tanjung Barat, Jakarta Selatan, Indonesia*

[7] *PT Mitra Mineral Megatama, Komplek Mitra Indah Utama 8 Pontianak, Kalimantan Barat, Indonesia*

[8] *Research Centre for Nuclear Fuel Cycle and Radioactive Waste Technology, The National Research and Innovation Agency (BRIN), Indonesia, ORCID https://orcid.org/0000-0003-2318-5098*

Abstract

The rising demand for scandium led to massive exploration activities for its discovery from mining by-products. Therefore, this study attempts to delineate the distribution of scandium-bearing minerals in the surrounding bauxite mining area, Tayan District, West Kalimantan Province, Indonesia. Preliminary studies were conducted by applying optical sensors to discriminate the types of minerals, such as kaolinite, gibbsite, goethite, and quartz. The spectral information aids the reconnaissance study by providing data on specific rocks and minerals using the short-wave infrared (SWIR), processed into a series of bands with spectral ranges from 0.35 to 2.5 μm. The data was then compared with the structural lineament from the ALOS PALSAR imagery to infer the prospective area with the structural pattern. The integrated band math minerals and geochemical data taken from X-ray fluorescence and Inductively Coupled Plasma-Mass Spectrometry suggest that the Sc-bearing minerals were disseminated predominantly on the bauxite laterite profile from pyroxene diorite and diorite parent rock weathering. The spectral range for goethite as the Sc-bearing minerals is from 0.43 to 1.03, with the main absorption features from 2.0 to. 2.4 . Furthermore, goethite is mainly concentrated at the top bauxite horizon associated with the structurally related hill. The ore-bearing minerals also occupied the tailing pond and some beneficiation areas in relatively minor proportion. This study is undoubtedly valuable for the practical need to support mineral exploration through remote predictive mapping.

Keywords:
scandium; goethite; Landsat; ALOS PALSAR; mapping

1. Introduction

The global demand for critical metals is significantly driven by technological innovation and the transition from fossil fuel to the zero-emission renewable energy system, such as electric vehicles, which requires a high-capacity storage system. One of the major forces in addressing the capacity challenges while considering the environment's safety and sustainability is the immediate recovery of critical metals. Scandium (Sc) metal is considered a critical substance due to its supply disruption. Therefore, it is imperative to conduct an exploratory study from by-product leach solutions in either nickel or bauxite refineries to determine the sediment residues in the beneficiation plant and vertical bauxite weathering profile. The idea of investigating the scandium-bearing minerals from bauxite mining operations is based on the ongoing feasibility studies in the Ural Mountains in Russia, which developed scandium recovery from the by-product of alumina refining (**USGS, 2019**).

The mineral exploration for Sc-bearing minerals in bauxite mining sites occupies large areas, combined with the limited cost of setting up geological field mapping. Remote sensing techniques are new approaches used to provide geological information, which aims to

Corresponding author: Rosmalia Dita Nugraheni
e-mail address: rosmalia.dn@trisakti.ac.id

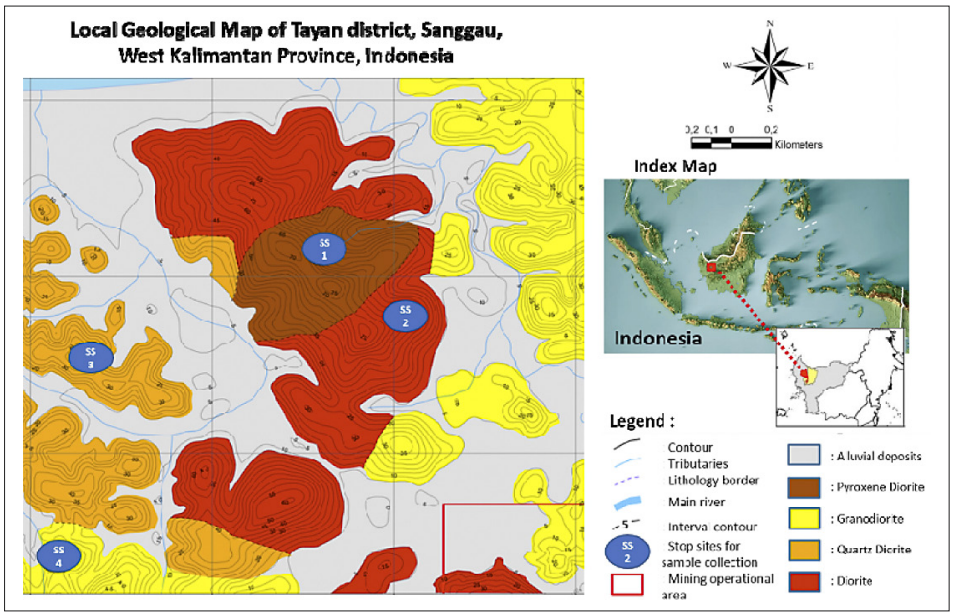

Figure 1: Local lithological units of the study area based on field mapping

delineate potential areas of the ore-bearing scandium in bauxite mining sites. The method is validated with geological field mapping, domaining of geochemical data, and ore-exploration to exemplify the potential area. A combination of field mapping and multispectral images can provide reliable results for the mineral mapping and further be proposed as the prospective area for scandium extraction.

Satellite images record vast geological and environmental features from various map scales. In examining regoliths, the visible to short wave infrared (SWIR) can map iron-rich minerals, clay, and associated residual bauxite occurrences (**Moghtaderi et al., 2017**). Minerals and rocks exhibit different spectral patterns due to distinct spectral absorption features (**Asadzadeh and de Souza Filho, 2016**). Preliminary studies applied multispectral imaging to measure the spectrum of light in each pixel (**Bruno et al., 2021; Calvini et al., 2019**) Landsat-8 OLI is used as a sensor consisting of eight channels or bands and broad spatial resolution (**Guerrero and Aleu, 2020**). Landsat imagery is powerful for gaining an overview of the environmental condition in large-scale mining (**Paull et al., 2006**). The spatial resolution of the light in each pixel is broken down into several different spectral bands to provide more information to the representative image. The greyscale or colour images can differentiate vegetation, water, soil, and various types of rock. More importantly, the processing image is primarily used to identify the target of ore-bearing scandium and associated minerals in bauxite ore. It is imperative to determine the iron minerals and mineral assemblages in bauxite for mineral exploration because it is gaining more attention since the method simply applies satellite technology. The technique is promising, inexpensive, and a quick tool for the initial assessment of surface to shallow surface conditions. However, no studies considered applying remote sensing to investigate and map the distribution of ore-bearing scandium in bauxite laterite.

According to literature studies, presently, there is no approach to map the scandium-bearing mineral, using satellite imageries for bauxite exploration. However, utilizing Landsat ETM+ imageries to investigate the relationship between bauxite indices and environmental factors (such as vegetation stress) has been performed in the Foumban area, Cameroon, and Nigeria (**Tematio et al., 2015**). The approach emphasizes the use of supervised classification and band ratio on Landsat ETM+ imageries to map the distribution of encrusted bauxitic surfaces. The study revealed the two categories of encrusted bauxitic surfaces, with thickness controlled by vegetation stress. A different approach has been performed to map bauxite alteration zone in Kolli Hills, Tamil Nadu, India, that utilised spatial and spectral information of VNIR and SWIR regions of ASTER data (**Lakshmi and Tiwari, 2018**). The method used in the study is called spectral unmixing by correlating the Normalized Difference Vegetation Index (NDVI) with alumina and vegetation fraction images and the structural density over DEM. NDVI is used to measure vegetation density as captured in satellite images. Their map depicted the lower alumina content as shown by a cyan and black colour, and the higher value of alumina content is notified by yellow.

1.1 Local Geological Setting

The local geological setting of the study area consists of five (5) lithological units, namely diorite, quartz diorite, granodiorite, pyroxene diorite, and alluvial deposits performed from field mapping (see **Figure 1**). The igneous rock units are mainly occupying the gentle hilly topography. In addition, the lithology is mainly identified as the poorly exposed rocks in the field due to intense

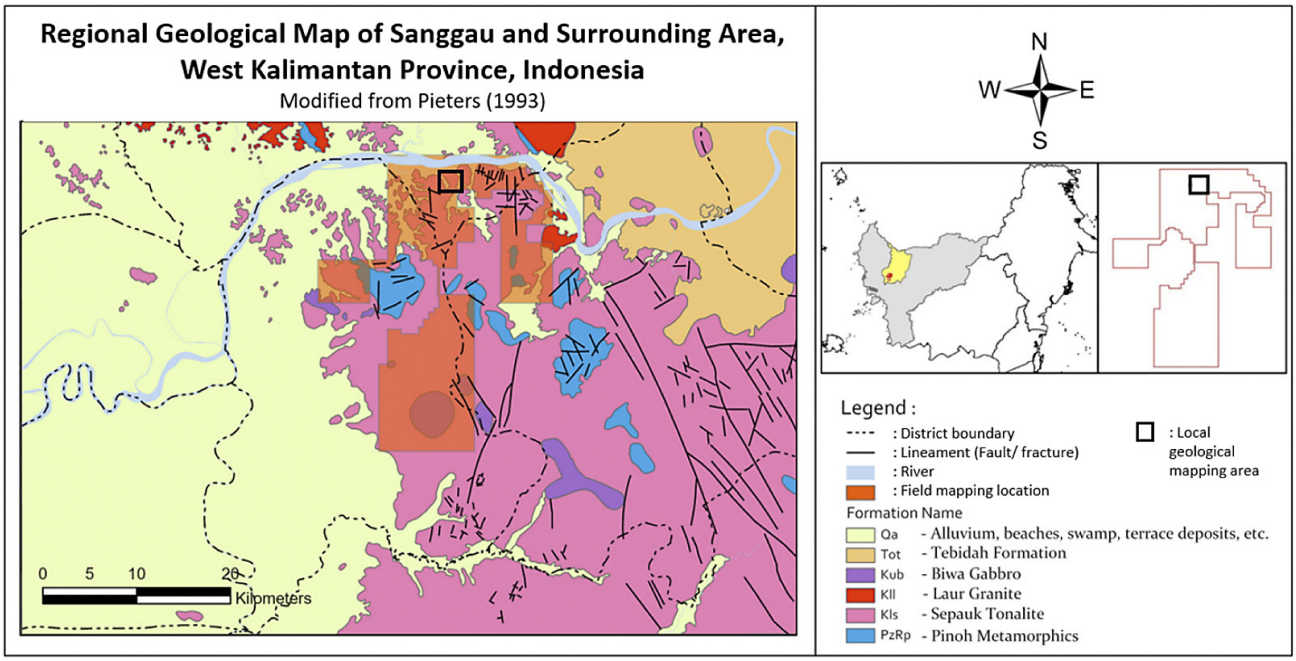

Figure 2: Regional geological map of the Tayan area, West Kalimantan Province, Indonesia (modified from **Pieters, 1993**)

weathering. Hence, it is an opportunity to optimise remote sensing utilization to complement this barrier.

The collected hand specimen samples were identified to determine the rock name. The igneous rocks exhibit equigranular, holocrystalline, medium-grained, and allotriomorphic to hypidiomorphic-granular. Megascopic examination for diorite indicates grey (fresh) to brownish grey (weathered) colour, with crystal size ranging from 2 to 4 mm. It has subhedral to anhedral textures and comprises predominantly plagioclase (40%-45%), indeterminate groundmass (38%-42%) with accessory minerals of hornblende (10%), subordinate biotite (5%), minor chalcopyrite as an altered mineral (1%) and opaque mineral (2%). Quartz diorite is like diorite with a sub-porphyritic and subhedral texture but contains quartz as an accessory mineral. Granodiorite exhibits a greater crystal size of 2 – 5 mm, it is hypidiomorphic-granular, and mineralogically consists of plagioclase (35%-40%), quartz (20%-25%), orthoclase (8%-10%), hornblende (8%-10%), biotite (5%) and groundmass (15%-18%). Pyroxene diorite is blackish grey, holocrystalline, has a crystal size of 1 to 4 mm, sub-porphyritic texture, composed of predominant plagioclase (30-35%), pyroxene (15%-18%) as an accessory mineral, with subordinate hornblende (5%-6%), occasional quartz (1%) and groundmass (42%-45%) as mineral constituents. The youngest alluvial deposit is brownish grey, contains granule to clayey-sized sediments, covers the older weathered rock, and mainly occupies the valley and lowland topography.

Various igneous rocks bodies indicate multiple intrusions occurred during the early Cretaceous period. In the later period, the area was subjected to a regional deformation and uplifting that led to the topography's dissection and laterite formation in gentle hills. The five lithological units in the study area (see **Figure 1**) belong to the Sepauk Tonalite Formation predominated by tonalite and granodiorite (see **Figure 2**) with subordinate monzogranite, quartz diorite, diorite, gabbro, quartz monzonite, and aplite. The Sepauk Tonalite Formation equals the Mensibau granodiorite, while the age determination was based on the K-Ar isotope analysis. The magmatism experienced complexity from the different petrogenetic stages during the early Cretaceous, such as periodic magma recharge and mixing with irregular boundaries (**Pieters, 1993**). The peripheral intrusion locally shows foliation, lineation, and recrystallization.

Information on the nature and age of the lithology or rock units must be considered when utilizing optical imagery for structural, lithological, and surficial mapping (**Harris et al., 2011**). The uplifting period in the late Cretaceous denotes that the rocks have been exposed and subjected to intensive weathering. Investigation and data collection on the fresh and weathered products in the vast areas will be time-consuming without remote sensing. Progressive weathering is generally associated with the formation of hydroxyl-bearing clays of illite, montmorillonite, and kaolinite due to hydrological leaching (**Heimsath et al., 2012**). The added value of utilizing the satellite image is the ability to diagnose the weathering (mineralogical change) by discriminating clays, quartz, and other secondary minerals. In addition, the broad spatial resolution of satellite images exhibits an extensive investigation of some external variables that contribute to the composition and architecture of the regolith, such as parent rocks, tectonics, landforms, and vegetation cover.

1.2 Spectral Properties for Minerals

Optical remote sensing with a moderate resolution of sensors is used to discriminate the rock and mineral types. The captured image in optical remote sensing is based on the reflected solar energy. The selected interval covers specific electromagnetic spectrum wavelengths, indicating that solar energy interacts differently with the atmosphere and the Earth's surface. The spectral range of electromagnetic radiation is within 0.45 – 0.69 μm, 0.76 – 0.90 μm, and 1.55 – 2.35 μm for bands 1 – 3, 4, and 5 – 7, also known as RGB, Near Infrared-NIR, and Short-wave infrared – SWIR, respectively (**Harris et al., 2011**). The visible and near-infrared are referred to as VNIR, with optical sensors characterized by a series of bands or channels. The spectral range can be used to evaluate mineralogical and lithological mapping since they exhibit different spectral patterns due to distinct spectral absorption features. Each mineral exhibits various electromagnetic spectral wavelengths concerning VNIR and SWIR response. As VNIR and SWIR have specific spectral ranges, the accuracy of the spectral range for mineral assemblage in bauxite is shown in **Table 1**. The accuracy denotes the response quality of VNIR and SWIR to diagnose each mineral. The response is clearly shown from the distinct spectral features of minerals at a particular wavelength. Overall, accuracy is critical before determining the composite band math.

The optical sensors also respond to the surface characteristics of the weathered residue; hence, the spectral signatures can be used to distinguish iron and clay weathering products. The iron oxides and hydroxides found in bauxite laterite include limonite and goethite. The iron minerals comprise distinct spectral absorption values in VNIR, ranging from 0.4 to 1.1 μm (**Peyghambari and Zhang, 2021**). Iron minerals containing Fe^{2+} and Fe^{3+} cations have an absorption peak of 1.03 (SWIR - band 5) and 0.64 μm (VNIR – band 4), respectively (**Peyghambari and Zhang, 2021**). Therefore, mapping Sc-bearing minerals in bauxite laterite employed the VNIR-SWIR region for alteration mineral mapping of Fe-OH and Al-OH minerals. In contrast, hydroxyl-bearing minerals, such as muscovite and clay minerals, have distinct spectral absorption in the SWIR region (mainly band 7), as shown in **Figure 3**. The reference spectral of minerals refers to the USGS spectral library of minerals and rocks from 0.35 to 2.5 μm regions (band 1 – 7) measured using lab, field, and imaging spectrometers (**Kokaly et al., 2017**).

Table 1: The accuracy of spectral analyses for each mineral in VNIR or SWIR **(Coulter, 2017)**

Type	Silicate Structure	Mineral Group	Mineral Name	VNIR Response	SWIR Response
Silicates	Sorosilicates	Epidote	Epidote	Non-diagnostic	Good
	Phyllosilicates	Mica	Muscovite	Non-diagnostic	Good
		Chlorite	Clinochlore	Non-diagnostic	Good
		Clay minerals	Illite	Non-diagnostic	Good
			Kaolinite	Non-diagnostic	Good
	Tectosilicates	Silica	Quartz	Non-diagnostic	Non-diagnostic
Non-silicates	Hydroxides		Gibbsite	Non-diagnostic	Good
	Oxides	Hematite	Hematite	Good	Non-diagnostic

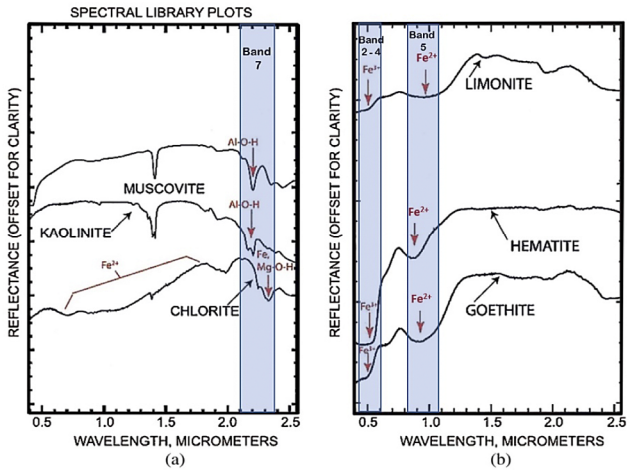

Figure 3: Spectral features of different mineral assemblages in bauxite that possible host the Sc metal, including (a) clay minerals and (b) iron oxides (modified from **Clark et al., 1993**)

2. Materials and Methods

2.1. Materials

In remote sensing, the data types utilise different spectral signals, including optical, synthetic aperture radar (SAR), microwave, LIDAR, and sonar data. The collective data used in this study consists of the optical sensors from Landsat and radar sensors from ALOS PALSAR. The Landsat data has a multispectral resolution to determine certain rock types and specific mineral compositions, such as iron and clay minerals. The spectral signals are produced from scattered and reflected sunlight. The images of Landsat-8 OLI (Operational Land Imager) used in this study were acquired from GloVis - USGS's Earth Explorer website (https://glovis.usgs.gov/app). The images covered the mining areas in Tayan District, Sanggau, West Kalimantan. They record the landscape on the earth's surface, including the outcrops,

tailing pond, and nearby morphological features. The Landsat image metadata shows an acquisition date on September 17th, 2019.

The radar sensor of ALOS (Advanced Land Observing Satellite) was also used to complement the shortage of cloud cover conditions, as seen in the optical sensor from the Landsat image. ALOS is equipped with the PALSAR sensor (Phased Array type L-band Synthetic Aperture Radar). The available SAR images in the studied area comprise the ALOS PALSAR Level 1.1 Complex, which was acquired from http://asf.alaska.edu. According to the image metadata, the acquisition date is August 10th, 2009, at 15:29:24Z. The advantage of using the SAR sensors is their four different polarization modes which allow for better image classification and target discrimination (**Mc Nairn and Brisco, 2004**)and thus remote sensing is an attractive approach to mapping and monitoring applications. Research performed with synthetic aperture radar (SAR. The polarization modes include HH – horizontal transmit and receive, HV – horizontal transmit and vertical receive, VH – vertical transmit and horizontal receive, and VV – vertical transmit and receive.

A total of 700 samples have been collected in the field and analysed using various analytical approaches in the laboratory. The samples include lateritic soils, crude and washed bauxites, clays, sediment residue, and red mud. They were taken from the exposed rocks, channel sampling in the pit, bauxite sediment residue from the beneficiation plant, and red mud from the tailing pond.

2.2. Methods

2.2.1. Pre-processing

Pre-processing stages for the satellite image have been performed for both Landsat and ALOS PALSAR. Optical imagery can be enhanced in many ways, such as by combining geoscience datasets and visually reproducing them in a GIS environment. Image processing using a computer helps undertake more quantitative analyses of the imagery for mineral mapping. This study used a multispectral sensor of Landsat-8 OLI to differentiate the ore-bearing minerals. Landsat imagery has been widely used in mining areas, including hydrothermal alteration, laterite, and residual deposits, because the sensors consist of 3 to 10 wider bands (**Behnia et al., 2012**). Some corrections and normalizations for the atmospheric effects were carried out in the initial image processing to gain an accurate surface condition and increase the clarity and acuity of the image. The initial processing method for Landsat OLI is radiometric correction, comprising radiometric calibration and atmospheric correction. The atmospheric effects appear due to dust, mist, aerosol scattering, and absorption of solar radiation capable of interfering with the reflectance of the detector (**Peyghambari and Zhang, 2021**). The atmospheric correction is performed using the FLAASH or Fast Line of Sight Atmospheric Analysis of Spectral Hypercubes. It starts by converting the digital number of images into radiance or applying the planetary reflectance approach from the top of atmosphere (TOA). This stage was applied to minimize distortions of an image due to the sensor shortage, which quantitatively interprets the data. Furthermore, the types of minerals were discriminated to process the composite band by analyzing the spectral cure of each mineral based on the USGS spectral library.

Data for the geological structures were obtained from SAR that primarily uses the advanced land observing satellite (ALOS PALSAR) type L-band SAR. Radiometric calibration was applied for the imaging process to increase the relative brightness and represent the surface reflection of the backscatter radar. The multi-looking stage was performed to improve the radiometric resolution, reduce the noise, and disentangle the image focus through speckle filtering. The image was then deskewed to return the data into the Doppler geometry, while terrain correction was finally used to rectify the geometric distortion. Image processing was performed using SNAP software for structural geological mapping, while the map layouts were mainly conducted using ArcMap and QGIS. The computed analysis was adopted from the studies conducted by **Harris et al. (2011), Leverington and Moon (2012), Tulcanaza and Meyer (2022), and Paull et al. (2006)** concerning the investigation of mineral and mining exploration. The lineament of the structural features can be identified by employing the principles of visual interpretation, such as shape and pattern. The structural information was mainly extracted from the exposed rocks or laterite products from the older and more complexly deformed igneous rocks. The ability to penetrate deeply into the subsurface makes SAR capable of detecting the buried target based on the physical soil properties **(Ghiyats Sabrian et al., 2017)**. Additionally, SAR can diminish the effect of atmospheric and vegetation cover that commonly obscures the structural information (**Dobrynchenko et al., 2018; Yonezawa et al., 2012**).

2.2.2. Band math mineral processing

This study used the SWIR spectral analyses to detect distinct mineral assemblages. Mineral mapping was created from the determination of surface composition. The absorption feature position from the multispectral satellite image was used to determine the various mineral chemistry, such as Al-Fe, in the forms of oxide and hydroxide. Most of the neomorphosed minerals (such as goethite, kaolinite) in bauxite laterite have distinct spectral features in VNIR-SWIR region.

The composite band math processes the raw images into the diagnosed minerals. The primary purpose of the composite band is to create the RGB colour from various bands, calculate the combination using different equations, select the appropriate colour composition according to the desired target, and make a new layer stacking

for raster data from numerous acquisitions time. One of the composite band math methods is utilizing the band math ratios, which differentates types of minerals by determining the digital number of each band pixel. **Clark et al. (1993)** determined a set of reference spectra in the USGS spectral library. The bands from the spectral library data of around 0.43 to 1.03 m, with important ferric iron detection in detachable bands 1 and 5 (**El-Mimouni et al., 2020; Hewson, 2020).** The spectral library was then used to discriminate mineral assemblages in bauxite, while the reflective spectral data characteristics used for Landsat 8 OLI in this study refers to **Rockwell et al. (2021)**, as shown in **Table 2**.

Table 2: Characteristics of reflective spectral data for Landsat 8 OLI (**Rockwell et al., 2021**)

Band	Wavelength Range (µm)	Band Center (µm)	Wavelength Region
1	0.43-0.45	0.44	Ultra+blue, coastal aerosol
2	0.45-0.51	0.48	Blue
3	0.53-0.59	0.56	Green
4	0.64-0.67	0.655	Red
5	0.85-0.88	0.865	Near Infrared (NIR)
6	1.57-1.65	1.61	Short-wave infrared (SWIR 1)
7	2.11-2.29	2.2	Short-wave infrared (SWIR 2)

Image processing of band math rationing was performed using ENVI 5.3 for mineral discrimination. In determining the composite band math, the ratios of mineral indices found in bauxite use a simple band ratio algorithm (**Drury, 1987**), wavelength range from **Rockwell et al. (2021)**, with some adjustments based on the spectral features from the spectral library. For clay mineral and iron-bearing minerals, the band ratio as follow (**Drury, 1987**):

$$\text{Clay minerals ratio} = \frac{\text{SWIR1}}{\text{SWIR2}} \quad (4)$$

Where:

SWIR1 – band 6,

SWIR2 – band 7.

The band ratio for ferrous minerals highlights iron-bearing minerals (including goethite) as follows:

$$\text{Ferrous minerals ratio} = \frac{\text{SWIR}}{\text{NIR}} \quad (5)$$

Where:

SWIR1 – band 6,

NIR – band 5.

The ratio algorithms above were modified according to the absorption spectral features on USGS spectral library, as seen in equations 6-9:

$$\text{Kaolinite} = \frac{\text{Band6}}{\text{Band7}} \quad (6)$$

$$\text{Gibbsite} = \frac{\text{Band5}}{(\text{Band6} + \text{Band7})} \quad (7)$$

$$\text{Goethite} = \frac{\text{Band3} + \text{Band6} + \text{Band7}}{\text{Band2} + \text{Band4} + \text{Band5}} \quad (8)$$

$$\text{Quartz} = \frac{\text{Band4}}{\text{Band7}} \quad (9)$$

The simple band math rationing results are displayed as the band math value from low to high. The band math value represents the relative abundance of minerals.

2.2.3. Mineral and geochemical analyses

The mineral analyses have been performed using conventional petrography and mineragraphy. Petrography examines the physical texture, structure, and mineral assemblages of the parent rocks and bauxites. Meanwhile, mineragraphy is primarily used to determine the assemblage of metal minerals, such as goethite, gibbsite, hematite, and hydrothermally altered pyrite mineral.

The geochemical data were collected from the exploration area, particularly from test pit locations. The geochemical analysis consists of X-ray fluorescence (XRF) and inductively coupled plasma-mass spectrometry (ICP-MS). X-ray fluorescence spectroscopy measures the concentration of Al_2O_3, Fe_2O_3, and $TSiO_2$ major elements. This analysis validates the accurate distribution of mineral composition in the studied area. The mineral map based on geochemical studies overlapped with the raster image from band math processing. Detailed scandium identification was performed using inductively coupled plasma-mass spectrometry (ICP-MS), with certain calibrators and quality control materials of OREAS as certified reference materials. The ICP-MS analysis includes 66 samples of lateritic soils, crude and washed bauxites, clays, sediment residue, and red mud.

2.2.4. Spatial Elemental Distribution Maps

The geochemical data were plotted as grades of the elemental map to infer the actual mineral distribution. The plotted major elements are Al_2O_3, Fe_2O_3, $RSiO_2$, and $TSiO_2$. Al_2O_3 is the major element that mainly constitutes gibbsite. Fe_2O_3 represents goethite as an iron-bearing mineral. $RSiO_2$ is reactive silica used to determine the SiO_2 derived from kaolinite clay minerals, while $TSiO_2$ is total silica that mainly constitutes quartz minerals.

The plots of geochemical data were carried out using the inverse distance weighted (IDW) method to estimate the ore grades at adjacent target locations. Inverse distance weighted (IDW) is known as one of the most common and simple geostatistical interpolation techniques

(**Jing and Wu, 2013; Kayıkçı and Kazancı, 2016**). The image and spatial data interpolations are essential to predict the target parameters in the field and develop the spatial distribution of certain ore-bearing minerals. This study uses the IDW method to interpolate the spatial distribution of gibbsite, goethite, kaolinite, and quartz minerals based on the grades of each prevalent major elements. In the IDW method, the grade values of the unsampled points are explicitly assumed to be more like the values of closer sampled points.

The principal method of IDW applies a linear-weighted combination set of sample points to determine grade value at the target location. The grade value at the target location will be assigned from the closest greater weight points. The equation is explained as follows (**Yang et al., 2020**)960 water samples were collected monthly along the Xin'anjiang River from 2008 to 2017. Twenty-four water quality indicators, according to the environmental quality standards for surface water (GB 3838-2002:

$$Z(So) = \sum_{i=1}^{n} WiZ(Si) \quad (10)$$

Where Z(So) is the unknown value at the target location of point So, n is the monitoring station, $Z(S_i)$ is the value at sampling location S_i, and W_i represents the weight or S_i grade value. The weight is defined using the following equation (**Yang et al., 2020**)960 water samples were collected monthly along the Xin'anjiang River from 2008 to 2017. Twenty-four water quality indicators, according to the environmental quality standards for surface water (GB 3838-2002:

$$Wi = \frac{\frac{1}{d_i^k}}{\sum_{i=1}^{n} \frac{1}{d_i^k}} \quad i = 1, 2, \ldots, n \quad (11)$$

Here, d_i represents the horizontal distance between the observed points and interpolation points, while k is the distance power. All interpolation calculations for IDW were performed using ArcGIS 10.2 software. The inputted data comprised coordination location, grade value for Al_2O_3, Fe_2O_3, $RSiO_2$, and $TSiO_2$ from the upper bauxite horizon, and 12.5 m for the distance of grid points. The grid point distance is selected based on the sample space. In the field, sampling has been performed every 25 m laterally from one test pit to another. Therefore, the grid point distance is half from the sample space or 12.5 in the calculation. Meanwhile, the IDW interpolation uses power two (2) since the variance is greater than 1. The distance calculation has also considered the gentle to wavy hill-sloping topography.

The interpreted band math value has been validated by combining the band math results with geochemical data from XRF and wet analysis, such as the grade of Al_2O_3, Fe_2O_3, $TSiO_2$, and $RSiO_2$. Practically, data validation for the mineral map has been performed by utilizing the band math images as the base map of each spatial elemental map. For instance, the band math images of gibbsite overlapped with the IDW plots of Al_2O_3, since gibbsite is mainly composed of Al_2O_3. A similar approach was done for band math goethite, which is used as the base map for Fe_2O_3, band math kaolinite as the base map plots of $RSiO_2$, and band math quartz as the base map plots of SiO_2. The grade of each major element was also presented in the low to high range.

2.3. Study Area

The study area focused on the surrounding bauxite mining site in the Tayan District, Sanggau, West Kalimantan, Indonesia, a region in the southern part of the Kapuas River. The study area is located in the equator line and based on the regional physiography, and it belongs to the Schwaner Block (**Bemmelen, 1949**). West Kalimantan is one of Indonesia's most significant resources and reserves of bauxite, situated on a tropical island with a high rainfall rate and dense vegetation. Bauxite is the primary source of aluminum ore production. Two alumina smelting plants were established in the study area. The preliminary geochemical studies conducted by **Nugraheni et al. (2021) and Putri et al. (2021)** revealed that the sediment residue resulting from bauxite beneficiation and red mud produced by the refinery process comprises scandium (Sc) and gallium (Ga) concentration. Therefore, with the evolution of this discovery, a regional study for mineral mapping should be performed to constrain the investigation area.

3. Results

2.1. Band math mineral

The spectra used to detect the mineral assemblages and create a mineral map range from 0.4 to 2.5 m, as shown in **Figure 4.** According to figure 4, kaolinite clay mineral mainly occupies lowland to gentle hill areas with dense vegetation cover. Clayey soil is identical to the plantation areas, which can be saturated by water. The gibbsite distribution has a similar pattern with kaolinite, indicating that kaolinite is present as neomorphosed mineral that constitutes the bauxite formation. Gibbsite or Al-OH-bearing minerals have a distinct absorption at 0.85 to 0.88 μm (band 5), 1.58 to 1.64 μm (band 6), and 2.15 to 2.22 μm (band 7). Fe-OH or goethite exhibits an absorption feature at 2.254 m and changes to 2.251 μm (band 7), relevant to the spectral patterns of **Kokaly et al. (2017)**. The changes in the absorption features of goethite are suspected to be related to bauxite texture from concretion to earthy. The distribution of goethite occupies the mining exploration, beneficiation, and tailing areas. In the exploration areas, the iron-bearing mineral of goethite predominantly occurs in steep terrain, marsh, and soil.

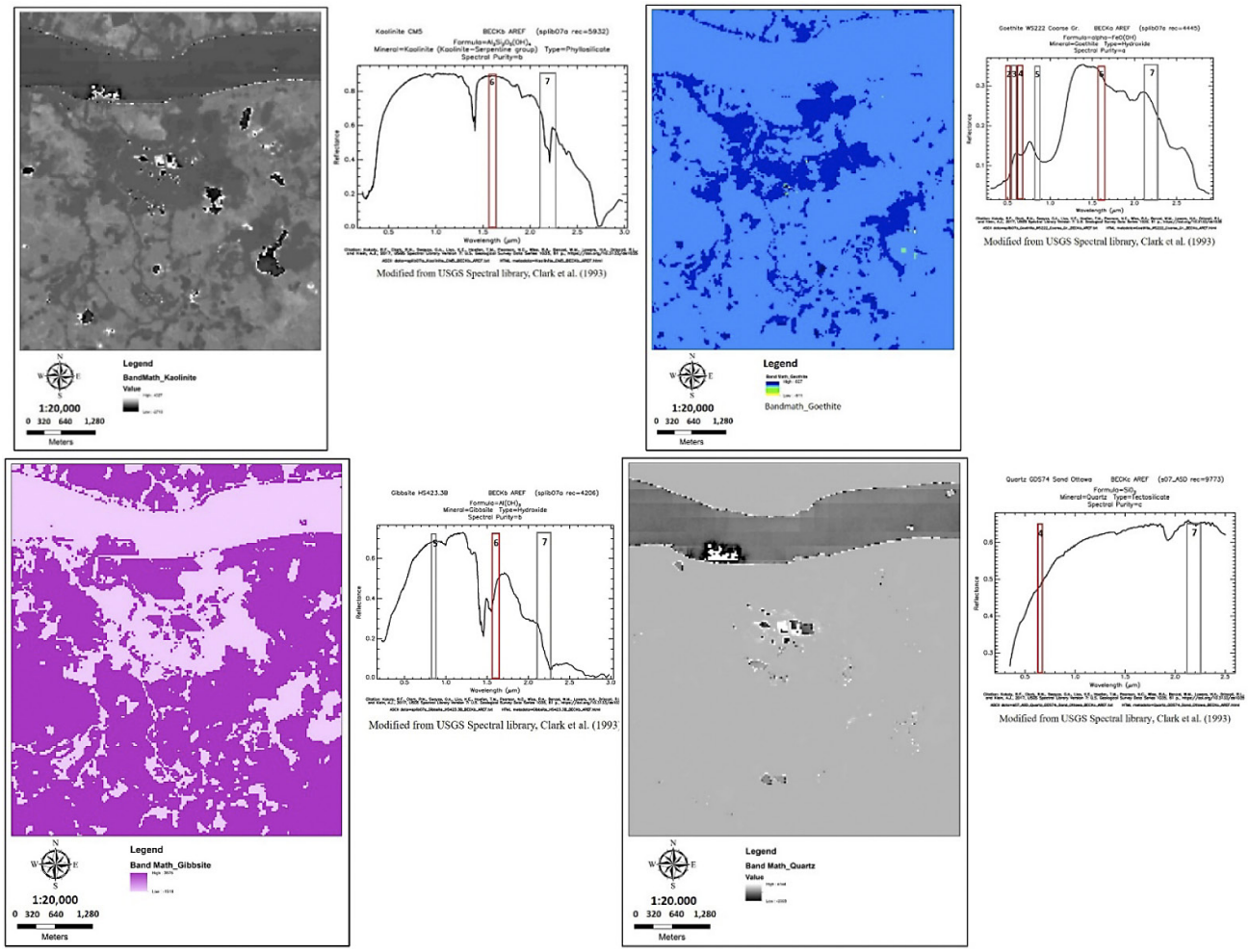

Figure 4: Mineral distribution map based on simple band rationing algorithm (SBR)

A combination of mineralogical maps based on remote sensing and the local geological map shows that kaolinite and quartz were mainly distributed in the alluvial deposits as denoted by high band value. Meanwhile, the rock exposures from granodiorite to diorite are mainly weathered to kaolinite, as shown by a variation in the range of moderate band value. A similar distribution pattern for kaolinite and gibbsite indicates that the parent rock contains abundant aluminosilicate minerals. The aluminosilicate minerals as the precursor minerals are primarily weathered to kaolinite followed by a prolonged weathering process to produce gibbsite. The distribution of goethite seems different from the three mineral assemblages. They are mainly associated with the weathering product of diorite and pyroxene diorite, as evidenced by high band value of goethite.

2.2. Faults and fractures detection using ALOS PALSAR

The genesis of bauxite laterite is associated with the structural deformation of uplift, faults, and fractures. The tectonic uplift exposed intrusive igneous rocks and further weathering to form bauxite laterite. Faults and fractures have also contributed to leaching and concentrating the critical metals in the bauxite horizon. These geological structures are well identified as lineaments under identification using interferometric SAR because SAR exhibits a high radio wave penetration capacity.

The main structural trends in **Figure 5** are NW-SE and NNE-SSW. The pattern of radial lines (green lines) indicates the occurrence of multiple intrusions which produce different rock characteristics. The multiple stages of magmatic intrusions generated different igneous rocks and mineral compositions as locally mapped in **Figure 1**. Dense lineaments suggest that the area underwent tectonic deformation, including the uplifting process of igneous rocks to the surface, which also drove the fault reactivation. High-density lineament associated with structural features potentially becomes a permeable zone to intensify the weathering process. However, in SAR processing, the roughness is not solely related to the structural geological features but also indicates the surface's acidity (pH) level (**Saepuloh et al., 2016**). Roughness in the southwest direction of the intrusion is subjected to the combination of the structural features and surface acidity as tailing materials are capable of

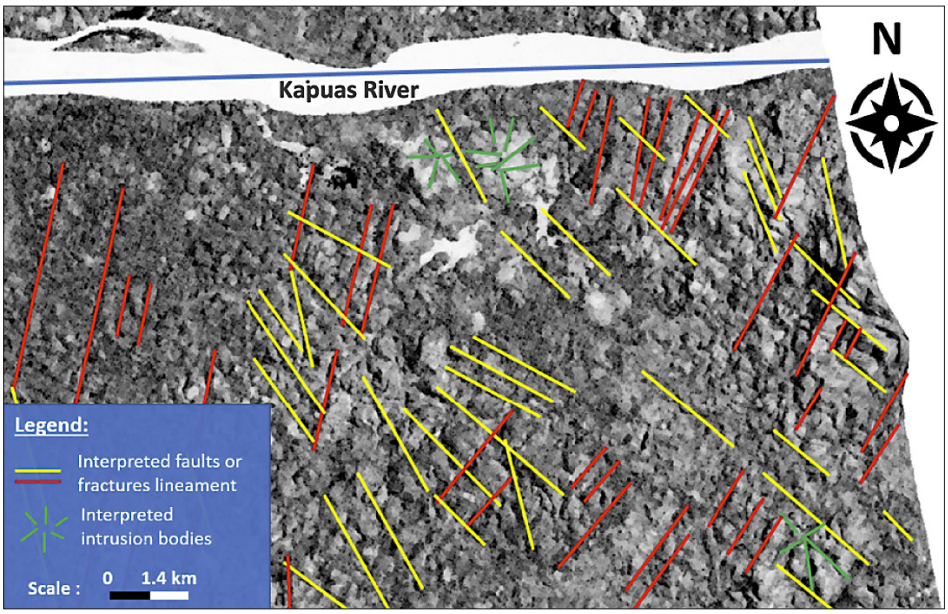

Figure 5: Lineament reconstruction based on ALOS PALSAR satellite imagery

contributing to the contamination of surrounding soils and groundwater.

2.3. Results of geochemical analysis and mineralogy

Multispectral remote sensing can detect minerals and represent them as a spectral pattern, which is then processed thoroughly to produce the mineral band math at a range of low to high. To validate the band math, the geochemical data has been performed accordingly from the upper (zone A), middle (zone B), and lower bauxite horizon (zone C). The geochemical data are plotted in the mineral distribution map to observe the reliability of remote sensing data. The bauxite geochemical data are summarized in **Table 3** for the XRF result and **Table 4** for the ICPMS result.

The concretion factor is the ratio of compacted bauxite concretion obtained after the washing process against the total weight of crude bauxite. The XRF results in **Table 3** show that the concretion factor controls the concentration of Al_2O_3 and Fe_2O_3 in bauxite samples. The results suggest that the concretion factor strongly correlates with the mineral assemblages in washed bauxite. Bauxite samples derived from pyroxene diorite have a higher concretion factor than other parent rocks. The bauxite characteristics from four different parent rocks also denote that pyroxene diorite and diorite tend to have higher grade of Fe_2O_3 and Al_2O_3. In contrast, bauxite derived from quartz diorite and granodiorite exhibits higher grades of SiO_2 and $RSiO_2$.

The precursor minerals in pyroxene diorite contain subordinate pyroxene and hornblende as accessory minerals. These primary minerals potentially altered to iron-oxide-hydroxide secondary minerals and increased the concentration of Fe_2O_3, as shown in **Figure 6**. The positive plot correlation of goethite mineral (Fe-O-OH) and scandium (Sc) strongly suggests that the scandium enrichment is associated with the presence of goethite as the Sc-bearing mineral. A similar positive bivariate plot has been depicted for gibbsite vs scandium concentration. However, the positive correlation is suspected due to iron encrustation on bauxite ore. A negative plot correlation between kaolinite vs scandium and quartz vs scandium implies that scandium has the poor capability to adsorb on the kaolinite surface or associate with quartz.

The information from mineralogy and geochemical data clearly emphasizes the focus of study to compare the band math mineral value from different parent rock domaining, including their bauxite mineral assemblage produced by the weathering of each parent rock. Based on **Table 3**, the highest concentration of Fe_2O_3, Al_2O_3, $TSiO_2$, and $RSiO_2$ is mainly found in the upper bauxite zone (zone A). Thus, geochemical plots for remote sensing validation mainly used the grade value from the A zone. Another distinct feature in **Table 3** displays that the elevated concentration of Fe_2O_3 will reduce the concentration of alumina (Al_2O_3). This result significantly justifies the mineral band value for gibbsite and goethite.

The scandium is mainly enriched and concentrated in the crude bauxite (upper zone or zone A) relative to parent rock. The ICPMS in **Table 4** documents the vertical geochemical profile of scandium from latosol to parent rock samples with an additional comparison between crude and washed bauxite and sediment residue products from each bauxite zone. Crude bauxite refers to ore bauxite obtained from a test pit, whereas washed bauxite refers to the crude bauxite that has been washed thoroughly to remove impurities. The washing process was performed in the beneficiation plant, and the residue was called sediment residue. The distinct feature from **Table 4** shows that the latosol or topsoil from the weathering of pyroxene diorite can concentrate more scandium com-

Table 3: Summary of geochemical data from XRF analysis

Sample Code	Bauxite zone	Thickness (m)	Sample space (m)	Concretion factor (CF; in %)	Al_2O_3 (%)	Fe_2O_3 (%)	$RSiO_2$ (%)	$TSiO_2$ (%)
Parent rock: Quartz diorite (**Figure 1**)								
E1	A	2.2	50	41.72	54.85	6.84	2.82	11.18
E28	A	2	50	45.26	44.84	5.59	4.25	25.57
E28	B	0.9	50	36.49	41.17	6.1	2.15	29.39
E153	A	2	25	69.7	52.47	9.29	3.47	0.55
E153	B	0.7	25	60	51.43	6.46	4.1	16.31
E228	A	2	25	43.7	47.63	4.85	4.25	25.25
E228	B	2	25	45	41.6	4.44	3.41	37.02
Parent rock: Pyroxene diorite **(Figure 1)**								
T100	A	2	25	70.2	37.5	35.12	0.97	2.33
T100	B	2	25	66.3	52.95	12.78	1.51	4.28
T100	C	2	25	50	45.77	19.6	2.53	8.54
T1003	A	2.2	25	69.4	50.09	17.79	0.99	2.66
T1043	A	2	25	63.6	48.78	17.73	2.03	5.35
T1043	B	1.8	25	58.9	48.06	14.43	2.43	11.17
T1076	A	2	25	65.2	32.31	34.52	2.06	13.18
T1076	B	1.4	25	66.6	40.76	21.98	2.5	14.27
Parent rock: Diorite **(Figure 1)**								
T1011	A	2	25	42.1	51.02	12.37	2.02	6.24
T1082	A	2	25	46.5	51.39	14.43	2.03	6.75
T1082	B	1.3	25	41.2	45.15	13.29	2.97	16.62
T1087	A	2	25	62.5	52.36	9.89	2.46	9.39
T1087	B	2	25	56	40.73	17.76	3.46	20.28
T1088	A	2	25	60.9	50.23	14.43	2.64	6.91
T1088	B	1.6	25	58.8	48.32	14.31	2.8	10.47
T133	A	2	25	48	52.37	11.71	2.2	6.82
Parent rock: Granodiorite **(Figure 1)**								
D01	A	2.3	25	57.6	43.98	6.72	3.92	28.39
D10	A	2.1	25	37.6	48.5	6.72	4.4	20.8
D100	A	2.1	25	50	48.75	5.23	4.24	22.62
D1004	A	1.9	25	51.8	48.18	6.09	4.16	22.41
D1007	A	2	25	46.8	51.85	5.28	2.8	16.67
D1007	B	0.6	25	42.3	39.87	4.87	2.38	38.89
D1008	A	2	25	42.1	48.42	5.16	3.67	23.15
D1008	B	2.2	25	40.4	46.95	5.76	3.85	24.87

pared to latosol from quartz diorite. The capability to concentrate scandium is associated with the presence of abundant organic litter as a vital carbon input in laterite paleosoil. Carbon tends to form covalent bonds with iron minerals and take up scandium during leaching. Meanwhile, the relative abundance of organic litter is linked to vegetation cover. As remote sensing data primarily records the spatial information from a surface, a careful selection procedure for geochemical data is essential to consider.

A correlation test of bivariate diagram has been performed to support the interpretation of the relationship between scandium towards other major elements. This diagram is to understand the behaviour between major elements and scandium during lateritisation (see **Figure 7**). The figure illustrates that the elevated concentration of scandium is linear to the increasing saturation of Al_2O_3 and Fe_2O_3. The beneficiation process has removed some of the encapsulated iron minerals on bauxite ore, leading to the depletion of Sc concentration in the washed bauxite sample. The positive correlation between Fe_2O_3 vs Sc indicates that scandium is preferentially to be incorporated into goethite. The incorporation of scandium into goethite structure occurred via isomor-

Table 4: Representative results for scandium concentration in various types of samples

Parent rock	Sample Code	Sample Type	Sc concentration (ppm)
Pyroxene diorite	T100	Latosol	41.9
	T100	Crude bauxite (Zone A)	53.3
	T100	Crude bauxite (Zone B)	42.6
	T100	Clay	39.4
	T100	Parent rock	15.1
	T100	Washed bauxite (Zone A)	52.6
	T100	Washed bauxite (Zone B)	47.6
	T100	Sediment residue (from bauxite zone A)	40.1
	T100	Sediment residue (from bauxite zone B)	32.6
Quartz diorite	E1	Latosol	29.6
	E1	Crude bauxite (Zone A)	44.3
	E1	Crude bauxite (Zone B)	33.1
	E1	Clay	24.4
	E1	Parent rock	11.7
	E1	Washed bauxite (Zone A)	42.9
	E1	Washed bauxite (Zone B)	31.1
	E1	Sediment residue (from bauxite zone A)	19
	E1	Sediment residue (from bauxite zone B)	23.7

phous substitution (**Qin et al., 2021**). Additionally, scandium is preferentially adsorbed on goethite surfaces (**Qin et al., 2021**). Meanwhile, the compatibility of gibbsite for the scandium uptake via ionic substitution seems debatable due to significant differences in the ionic radii.

2.4. Elemental mapping applied to band math mineral

The elemental distribution map is applied to band math mineral map to validate the surrounding mining area, since the data for elemental map were collected from the bauxite test pit (as shown in **Figure 8**). Both mineral band math and plotted geochemical data were depicted from low to high value. The value represents the relative abundance of the ore-bearing minerals distributed in the studied areas. Validation results show different performances for each mineral map. From **Figure 8,** high-grade Al_2O_3 obtained from XRF analysis mainly occupied the low gibbsite band math, with an occasional presence in the high band math value. This validation result suggests that a slight distribution of gibbsite as observed using satellite images potentially yielded by high-grade alumina. In contrast, the abundant distribution of quartz mainly exhibits low-grade silica for the bauxite-derived from diorite and pyroxene diorite and low to moderate grade silica for the bauxite derived from quartz diorite and granodiorite.

A proper trend of the mineral abundance and the grade value was shown for goethite and kaolinite. The high to moderate grade of Fe_2O_3 mainly occupied the moderate to high band math value of goethite in many laterite outcrops. An exclusion occurred in the surrounding tailing and washing plant. A contrast overlaid data of moderate value of goethite band math, and low-grade Fe_2O_3 revealed iron oxide-hydroxide contaminants from the acid refinery process in bauxite. A proper fitting of kaolinite band math to $RSiO_2$ grade indicates that band math value is valid to determine the distribution of kaolinite either in outcrops or tailing areas.

2.5. Mineral mapping in bauxite laterite and surrounding mining areas

The mining concession includes the exploration and production areas, tailing pond, sediment residue pond, and refinery plant. Domaining the surrounding mining sites is essential to manifest the target area through the collection of the exploration area. This process uses the spatial patterns of the mineral assemblage to generate the distribution of Sc-bearing minerals and other mineral assemblage found in bauxite laterite.

As the weathering process occurs vertically and laterally, information about the parent rocks and the vertical weathering profile is important to determine the distribution map of the ore-bearing Sc. In the vertical weathering profile of bauxite, goethite occupies the top bauxite horizon that commonly contains ferricrete and abundant spherical bauxite concretion texture. The bigger concretion texture is bigger than the earthy bauxite. The bigger concretion occupies the top and gradually changes to an earthy texture on the lowest horizon. Thus, geochemical data from the top bauxite horizon is primarily used to plot the grades of Fe_2O_3. The mineral mapping for the ore-bearing Sc is acquired from band math validation of goethite to determine the accuracy of the interpreted goethite band math due to the limited scandium data. In the 2D mineral map, the results suggested that goethite or secondary iron mineral and the Sc-bearing mineral were disseminated in moderate to high-value band math of goethite, as shown in **Figure 9.** Goethite distribution is mainly associated with gibbsite, despite having a contrast enrichment pattern of high-grade goethite, which corresponds to a moderate grade of bauxite and vice versa (see **Figure 9**).

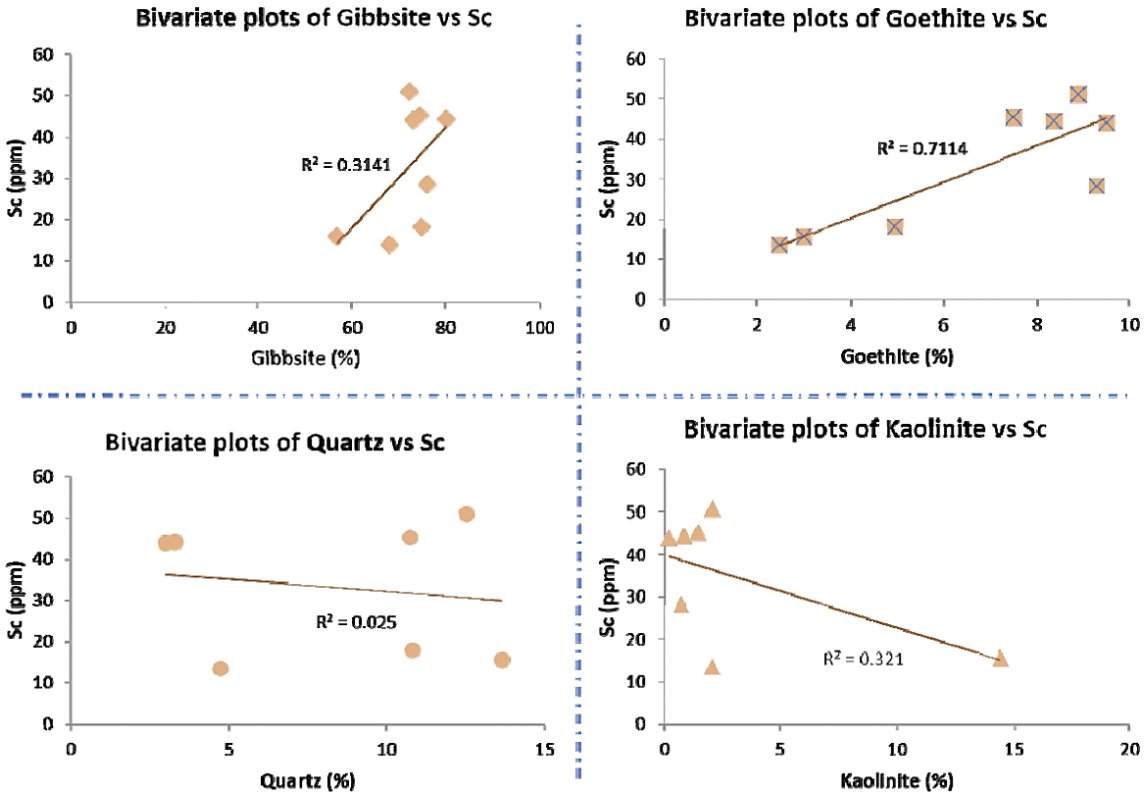

Figure 6: Bivariate plots depicting scandium concentration in association with gibbsite, goethite, quartz, and kaolinite minerals.

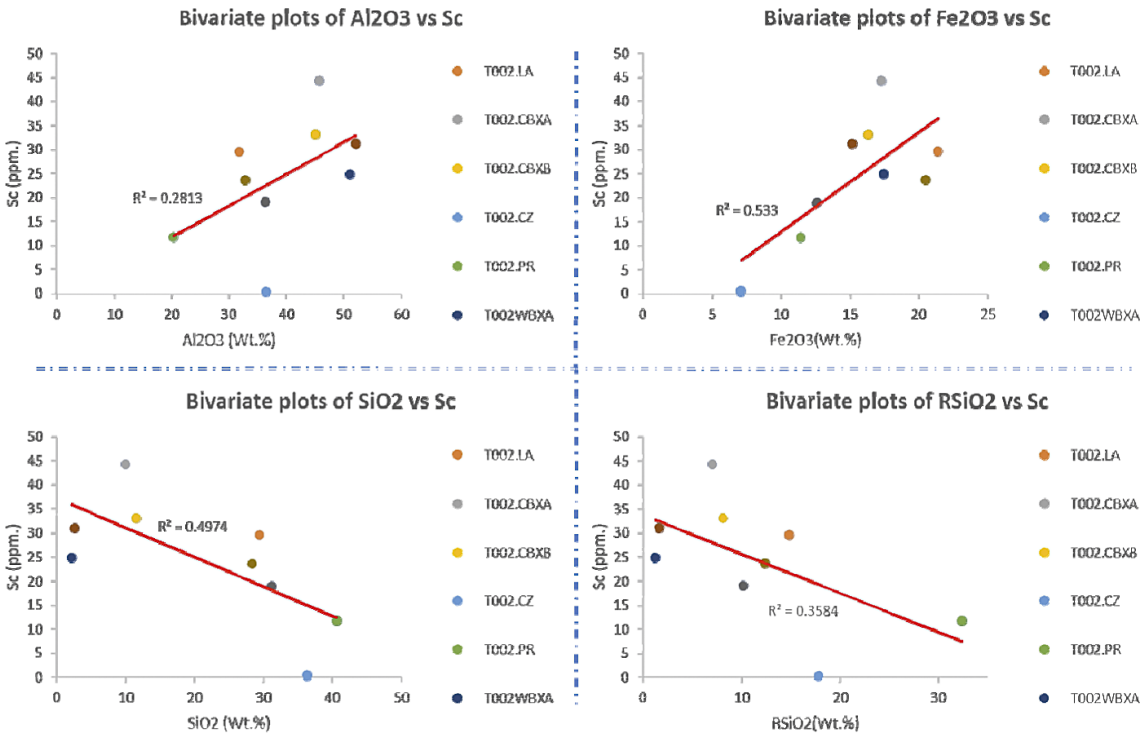

Figure 7: Bivariate plots depicting scandium concentration and covariation trends with Al_2O_3, Fe_2O_3, $TSiO_2$, and $RSiO_2$ major elements. Samples were collected vertically from test pit, from top to bottom consist of LA- latosol; CBXA-crude bauxite from the upper bauxite zone (A zone); CBXB-crude bauxite from the lower bauxite zone (B zone); CZ-samples from clay zone; PR- rock samples from parent rocks. Additional samples of WBXA- washed bauxite from A zone were used to compare with the crude samples.

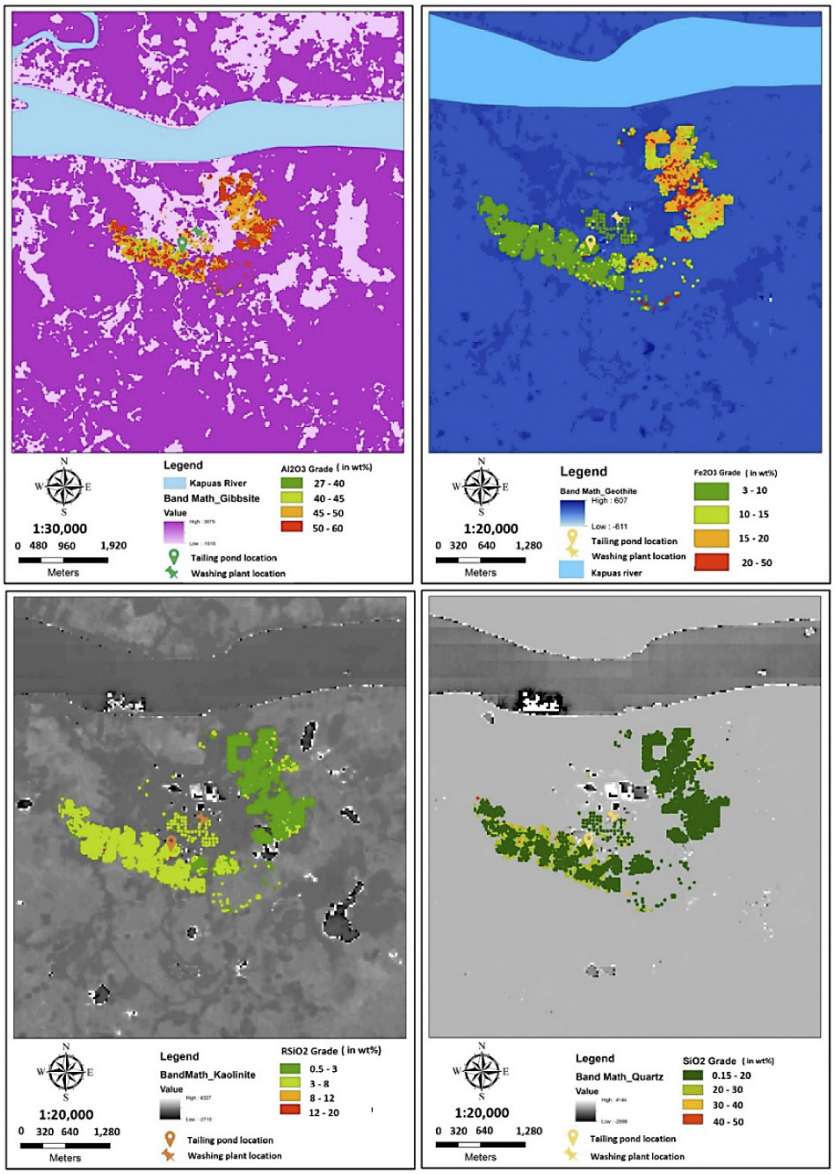

Figure 8: Mineral map reconstruction from a combination of spectral enhancement products using Landsat-OLI 8, field geological mapping, and geochemical data.

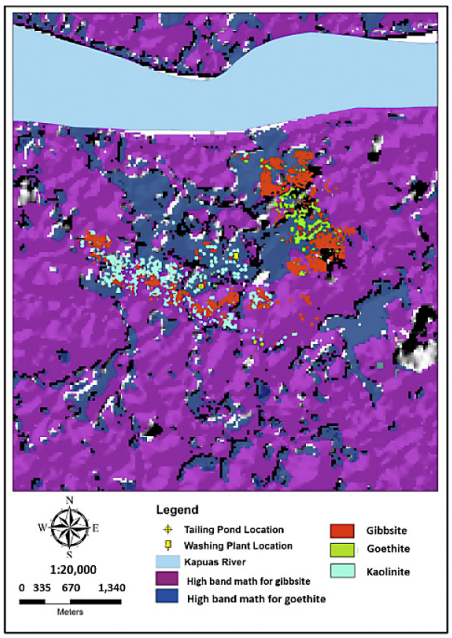

Figure 9: Spatial distribution of goethite as Sc-bearing mineral and bauxite assemblage minerals around Tayan areas

The group plots of gibbsite and kaolinite in **Figure 9** evidenced that the gibbsite formation is associated with the neomorphism of kaolinite. The assemblage minerals suggest that their presence is derived from their precursor minerals' leaching and enrichment processes in parent rocks. Thus, the abundant distribution of gibbsite and kaolinite plots denotes that their parent rock is felsic to intermediate in composition. Kaolinite is also disseminated in the washing plant, tailing pond, and along the lowland areas nearby the refinery plant. In contrast, the goethite distribution is slightly found in the surrounding washing plant and tailing pond, which contains 3-15 wt% of Fe_2O_3. Apart from this approach, field visits and sample collection are still effective in validating the classified mineral map.

4. Discussions

West Kalimantan is known for the existence of a bauxite belt that stretched NW-SE from the Singkawang to Kendawangan areas. The bauxite deposit in the province is mainly related to the intense paleo-weathering of igneous parent rock during the Cretaceous period. The bauxite deposit comprises diagnostic alteration patterns with distinctive minerals, which depend significantly on the types of parent or source rocks.

Bauxite deposits occurred during the fundamental genetic process of bauxitisation (see **Figure 10**), reliant on the parent rock's external controlling factors, such as physiochemical condition of the parent rock, temperature, tectonic, hydrology, and topography. Bauxite later-

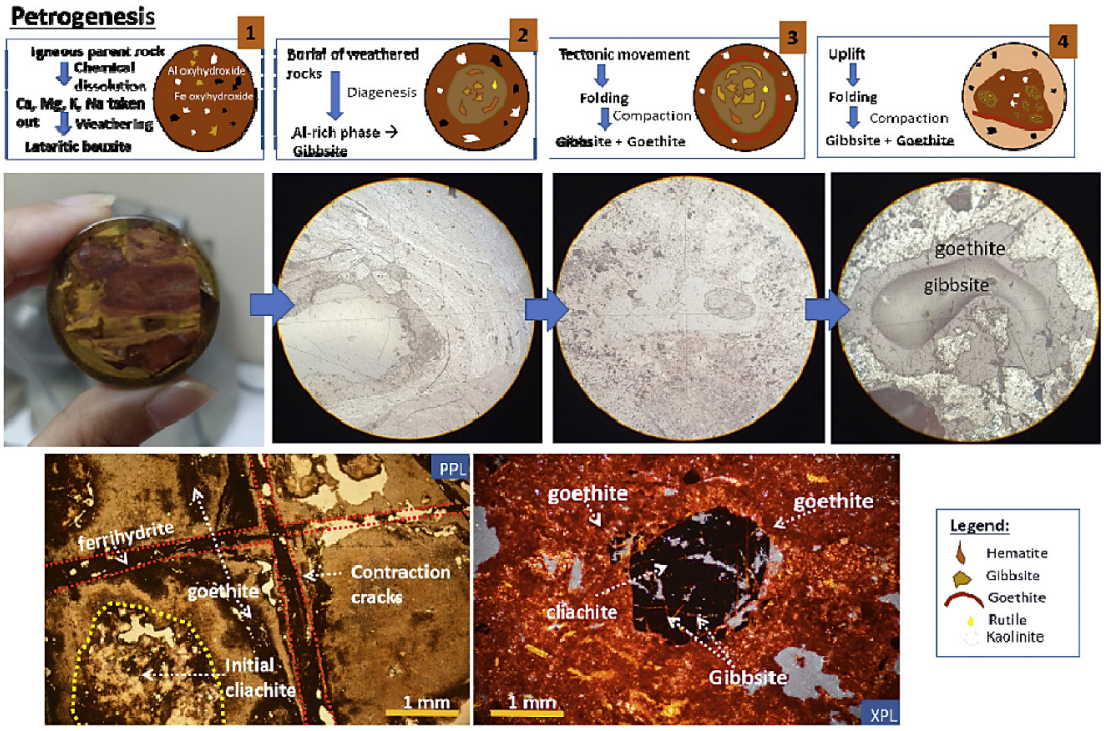

Figure 10: A schematic illustration of bauxite ore petrogenesis based on a diagnostic of its concretion to pisolite texture and mineral assemblage. Petrogenesis was interpreted from the collective laboratory examination for mineragraphy (middle photomicrographs) and thin section petrography (lower photomicrographs). Lower thin section photos were taken from **Nugraheni et al. (2021)**

ites are mainly produced in tropical geographic areas by weathering, which enriches alumina, iron, and trace elements of scandium and gallium (**Nugraheni et al., 2021**). The enrichment of scandium corresponds to the ionic substitution with Fe^{3+} in a goethite crystal structure or adsorption on a crystal surface. Multispectral remote sending is essential to determine the mineral composition in the bauxite mining site and delineate its distribution for exploring scandium-bearing minerals.

According to the schematic illustration in **Figure 10**, the early stage of weathering is the formation of contractional cracks that enlarge along the intense weathering process. Ferrihydrites [Fe_5HO_8, $4H_2O$] are mainly filled cracks, while cliachite or colloidal aluminum hydroxides constitute most bauxite ore formed in the core between the contraction cracks. Transformation of gibbsite nucleation until goethite encapsulation is clearly observed under the reflected light microscope (middle photos of **Figure 10**) and polarized light microscope (lower photos of **Figure 10**). Parent rocks predominantly composed of plagioclase are used to generate an abundant Al-rich phase during weathering, while ferromagnesian minerals, which occasionally present as an accessory mineral, contribute to enveloping the bauxite ores during further tectonic and compaction stages. The relict or resistant minerals, namely rutile, quartz, trace ilmenite, and sphene, initially occurred during the burial of weathered rocks together with neogenetic minerals, including kaolinite, gibbsite, goethite, and hematite. Gibbsite nucleation occurred progressively with the formation of goethite. Therefore, the maximum enrichment of the Sc-bearing minerals (goethite) and bauxite ore (gibbsite) occurred at the top of the bauxite horizon. The petrogenesis study was used to determine and justify the geochemical data overlaid with band math from the satellite image processing. This study is ultimately used to generate a mineralogic map, particularly the distribution of Sc-bearing minerals in the study area.

A combination of the interpreted structure (see **Figure 5**), geological rock unit (see **Figure 2**), and mineral mapping suggests that parent rock-related intrusion bodies separated by the interpreted fault exhibit different magma compositions. Variability of the magma composition depends on the magma supply, mixing, and interaction with the country rocks. The magma composition contributes to the presence of iron minerals as the host mineral for scandium. The intrusion bodies in the southern part of Kapuas River to the east predominantly contain decomposed diorite and pyroxene diorite rocks. To the west of the intrusion body, the bauxite weathering profile is derived from granodiorite and quartz diorite, exhibits a moderate band math value of goethite, and indicates that Sc-bearing minerals are only in minor proportion.

This study is used as a proxy to determine the prospect of utilizing tailing and sediment residue materials for scandium extraction in the future. Based on the mineral distribution map in the surrounding tailing areas, it

can be inferred that goethite primarily occupies the tailing pond and beneficiation areas despite having a minor concentration. The plotted geochemical data distributed around the tailing pond and bauxite washing plant shows that the iron oxide grade ranges from 5 to 15 wt%. High-grade iron minerals are mainly disseminated within the bauxite laterite derived from diorite. On the contrary, kaolinite is distributed widely around the tailing pond, washing plant, and laterite outcrop derived from quartz diorite and granodiorite weathering. A similar distribution has been shown for the quartz mineral, in which abundant quartz ($TSiO_2$) is associated with the low-grade bauxite derived from quartz diorite. The delineated areas relating to the emplacement of Sc-bearing minerals are structurally located in association with intrusion bodies and faulted zones. Finally, it is essential to characterize the mineralogy in the exploration and beneficiation areas. The beneficiation area is generally used to emplace the sand and clay materials separated from the bauxite ore through washing treatment. Utilizing remote sensing for mineral mapping, we can consider using tailing and washing plants to recover scandium.

The geological information provided in this study is significantly dependent on the spatial resolution of the sensor with any form of bias subjected to the sensor resolution and the atmospheric correction. Landsat exhibits 30 m resolution for multispectral bands (**Harris et al., 2011**); hence, this study is preferentially useful for regional mapping that offers information on mineralogy, lithology, structure, and infrastructure for field planning. In detail, this preliminary study guided constraining the investigated area before estimating the scandium resources and recovering the metals for the future.

5. Conclusion

Multispectral remote sensing is a promising mineral exploration, lithological, and lineament mapping technique. Mineral mapping depicts the distribution of relict and neomorphosed minerals found in bauxite, such as quartz, gibbsite, goethite, and kaolinite. The distribution of mineral assemblages has been interpreted from the combination of datasets containing band math of various grade plots, such as $TSiO_2$, Al_2O_3, Fe_2O_3, and $RSiO_2$. The most valuable bands used to detect the goethite as Sc-bearing minerals are from the SWIR region or around 0.43 to 1.03 μm, with the main absorption features at 2.0 to 2.4 μm. The spectral range used for band math processing has been generated from the USGS spectral library of minerals and rocks, with wavelengths ranging from 0.35 to 2.5 μm regions. Goethite is mainly accumulated in the structurally related gentle hill topography with the weathering profile, mostly found at the top bauxite horizon. The moderate to high proportion of goethite as interpreted from the combination of band math and plotted geochemical data is commonly associated with the weathering of diorite and pyroxene diorite igneous parent rock. Goethite, which mainly occurred in a minor proportion as evidenced from the composite band math, was concentrated in the beneficiation areas, and tailing ponds. However, a minor proportion of goethite does not indicate that it contains low-grade scandium since most of the high-grade precious metal was also recovered from the low tonnage. Further laboratory examination must be considered for the scandium extraction from the tailing pond and beneficiation areas. However, priority should be taken for every bauxite washing and refinery process derived from diorite and pyroxene diorite source rocks. Multispectral remote sensing, combined with the nature of geological information, acts as a proxy to map the Sc-bearing minerals for reconnaissance study. Future studies need to develop a technique for remote predictive mapping.

Acknowledgement

The authors are grateful to the research institution of Universitas Trisakti (LPPM) for funding this study. We would also like to express gratitude to the editors, anonymous reviewers, and readers for their constructive comments.

6. References

Asadzadeh, S., de Souza Filho, C.R. (2016): A review on spectral processing methods for geological remote sensing. International Journal of Applied Earth Observation and Geoinformation, 47, 69–90. doi: 10.1016/j.jag.2015.12.004

Behnia, P., Harris, J.R., Rainbird, R.H., Williamson, M.C., Sheshpari, M. (2012): Remote predictive mapping of bedrock geology using image classification of Landsat and SPOT data. International Journal of Remote Sensing, 33, 6876–6903. doi: 10.1080/01431161.2012.693219

Bemmelen, R.W. van (Reinout W. van) (1949): The geology of Indonesia / R.W. van Bemmelen. Govt. Printing Office, The Hague.

Bruno, R., Kasmaeeyazdi, S., Tinti, F., Mandanici, E., Balomenos, E. (2021): Spatial component analysis to improve mineral estimation using sentinel-2 band ratio: Application to a Greek bauxite residue. Minerals, 11. doi: 10.3390/min11060549

Calvini, R., Ulrici, A., Amigo, J.M. (2019): Chapter 3.9 - Growing applications of hyperspectral and multispectral imaging. In: Amigo, J.M. (Ed.), Hyperspectral Imaging, Data Handling in Science and Technology. Elsevier Publ. Co., 605–629.

Clark, R.N., Swayze, G.A., King, T.V. V, Gallagher, A.J., Calvin, W.M. (1993): The US Geological Survey, digital spectral reflectance library: Version 1: 0.2 to 3.0 microns. In: JPL, Summaries of the 4th Annual JPL Airborne Geoscience Workshop. Volume 1: AVIRIS Workshop.

Coulter, D. (2017): Advances in Spectral Geology and Remote Sensing : 2008 – 2017 25. In: Proceedings of Exploration 17: Sixth Decennial International Conference on Mineral Exploration, 23–50.

Dobrynchenko, V., Kokorinand, I., Shebalkova, L. (2018): Application of synthetic aperture radars for the ground displacement monitoring in mineral mining areas. IOP Conference Series: Earth and Environmental Science, 134, 012013. doi: 10.1088/1755-1315/134/1/012013

Drury, S.A. (1987): Image Interpretation in Geology, 2009/05/01. ed, London: Allen and Unwin. Cambridge University Press.

El-Mimouni, M., Aarab, A., Lakhloufi, A., Hamzaoui, A., Akhssas, A., Benyas, K. (2020): Contribution of multispectral remote sensing to mining exploration in the Rehamna Massif, Moroccan Meseta. E3S Web of Conferences, 150, 1–13. doi: 10.1051/e3sconf/202015003018

Ghiyats Sabrian, P., Saepuloh, A., Syafrizal, Naftali Hawu Hede, A. (2017): Identification of Altered Minerals Based on Synthetic Aperture Radar (SAR) for Mineral Exploration in a Tropical Area. IOP Conference Series: Earth and Environmental Science, 71. doi: 10.1088/1755-1315/71/1/012021

Guerrero, G.B., Aleu, A.L. (2020): Hyper- and multispectral image analysis methods for mineral identification: two cases of study.

Harris, J.R., Wickert, L., Lynds, T., Behnia, P., Rainbird, R., Grunsky, E., McGregor, R., Schetselaar, E. (2011): Remote predictive mapping 3. optical remote sensing - a review for remote predictive geological mapping in northern canada. Geoscience Canada, 38, 557–584.

Heimsath, A.M., DiBiase, R.A., Whipple, K.X. (2012): Soil production limits and the transition to bedrock-dominated landscapes. Nature Geoscience 5, 210–214. doi: 10.1038/ngeo1380

Hewson, R.D. (2020): Status and Developments in Geological Remote Sensing. Fast Times, 25, 54–66.

Jing, M., Wu, J. (2013): Fast image interpolation using directional inverse distance weighting for real-time applications. Optics Communications, 286, 111–116. doi: 10.1016/j.optcom.2012.09.011

Kayıkçı, E.T., Kazancı, S.Z. (2016): Comparison of regression-based and combined versions of Inverse Distance Weighted methods for spatial interpolation of daily mean temperature data. Arabian Journal of Geosciences, 9. doi: 10.1007/s12517-016-2723-0

Kokaly, R.F., Clark, R.N., Swayze, G.A., Livo, K.E., Hoefen, T.M., Pearson, N.C., Wise, R.A., Benzel, W.M., Lowers, H.A., Driscoll, R.L., Klein, A.J. (2017): USGS SPectral Library Version 7, U.S. Geological Survey. Reston, Virginia. doi: 10.3133/ds1035

Lakshmi, S.V., Tiwari, R. (2018): Mapping of bauxite ore using remote sensing and gis. International Journal of Pure and Applied Mathematics, 119, 3367–3375.

Leverington, D.W., Moon, W.M. (2012): Landsat-TM-based discrimination of lithological units associated with the Purtuniq ophiolite, Quebec, Canada. Remote Sensing, 4, 1208–1231. doi: 10.3390/rs4051208

Mc Nairn, H., Brisco, B. (2004): The application of C-band polarimetric SAR for agriculture: A review. Canadian Journal of Remote Sensing, 30, 525–542. doi: 10.5589/m03-069

Moghtaderi, A., Moore, F., Ranjbar, H. (2017): Application of ASTER and Landsat 8 imagery data and mathematical evaluation method in detecting iron minerals contamination in the Chadormalu iron mine area, central Iran. Journal of Applied Remote Sensing, 11, 1–22. doi: 10.1117/1.JRS.11.016027

Nugraheni, R.D., Riyandhani, C.P., Apriniyadi, M., Sunjaya, D. (2021): Critical raw materials enrichment in bauxite laterite: a case study of diverse parent rock types. IOP Conference Series: Earth and Environmental Science, 882, 012024. doi: 10.1088/1755-1315/882/1/012024

Paull, D., Banks, G., Ballard, C., Gillieson, D. (2006): Monitoring the environmental impact of mining in remote locations through remotely sensed data. Geocarto International, 21, 33–42. doi: 10.1080/10106040608542372

Peyghambari, S., Zhang, Y. (2021): Hyperspectral remote sensing in lithological mapping, mineral exploration, and environmental geology: an updated review. Journal of Applied Remote Sensing, 15, 1–25. doi: 10.1117/1.JRS.15.031501

Pieters, P.E. (1993): Geologi Lembar Pontianak/Nangataman, Kalimantan = Geology of the Pontianak/Nangataman Sheet area, Kalimantan / oleh (by) P.E. Pieters & P. Sanyoto. Pusat Penelitian dan Pengembangan Geologi, Bandung.

Putri, A.R.K., Setijadji, L.D., Sunjaya, D. (2021): Potential Enrichment of Scandium in Bauxite Deposit for the Emerging Green Technology Needs. Indonesian Journal of Economic Geology, 1, 72–84. doi: 10.51835/ijeg.2021.1.1.343

Qin, H.B., Yang, S., Tanaka, M., Sanematsu, K., Arcilla, C., Takahashi, Y. (2021): Scandium immobilization by goethite: Surface adsorption versus structural incorporation. Geochimica et Cosmochimica Acta, 294, 255–272. doi: 10.1016/j.gca.2020.11.020

Rockwell, B.W., Gnesda, W.R., Hofstra, A.H. (2021): Improved Automated Identification and Mapping of Iron Sulfate Minerals, Other Mineral Groups, and Vegetation using Landsat 8 Operational Land Imager Data, San Juan Mountains, Colourado, and Four Corners Region. Reston, Virginia.

Saepuloh, A., Koike, K., Heriawan, M.N., Kubo, T. (2016): Quantifying Surface Roughness to Detect Geothermal Manifestations from Polarimetric Synthetic Aperture Radar (PolSAR) Data.

Tematio, P., Meli Songmene, S., Leumbe Leumbe, O., Momo Nouazi, M., Yemefack, M., Yongue Fouateu, R. (2015): Mapping bauxite indices using Landsat ETM+ imageries constrained with environmental factors in Foumban area (West Cameroon). Journal of African Earth Sciences, 109, 47–54. doi: 10.1016/j.jafrearsci.2015.05.010

Tulcanaza, E., Meyer, H. (2022): Applicability of multispectral Sentinel data for mineral exploration by use of remote sensing and geospatial technologies A case study in Northern Chile. Institut für Geoinformatik der Universität Münster.

USGS (2019): Mineral Commodity Summaries. 1(703): 2019-20.

Yang, W., Zhao, Y., Wang, D., Wu, H., Lin, A., He, L. (2020): Using principal components analysis and idw interpolation

to determine spatial and temporal changes of Surfacewater quality of Xin'Anjiang river in huangshan, china. International Journal of Environmental Research and Public Health, 17, 1–14. doi: 10.3390/ijerph17082942

Yonezawa, C., Watanabe, M., Saito, G. (2012): Polarimetric decomposition analysis of ALOS PALSAR observation data before and after a landslide event. Remote Sensing 4(8):2314-28. doi: 10.3390/rs4082314

SAŽETAK

Multispektralno daljinsko očitavanje područja distribucije minerala sa sadržajem skandija u rudnicima boksita pokrajine Zapadni Kalimantan, Indonezija

Rastuća potražnja za skandijem dovela je do velikih istraživanja sa svrhom njegova otkrivanja na jalovištima rudarskih postrojenja. U radu se prikazuje distribucija minerala sa sadržajem skandija u okolici rudnika boksita u okrugu Tayan, provincija Zapadni Kalimantan, Indonezija. Provedeno je preliminarno istraživanje primjenom optičkih senzora za razlikovanje minerala kao što su kaolinit, gibsit, getit i kvarc. Spektralni podatci prospekcije daju informacije o specifičnim stijenama i mineralima pomoću infracrvenoga (SWIR) kratkog vala, obrađenoga u niz traka sa spektralnim rasponima od 0,35 do 2,5 μm. Podatci su zatim uspoređeni sa strukturnim lineamentima iz slika ALOS PALSAR kako bi se otkrilo perspektivno područje s obzirom na strukturni sklop. Skup minerala, matematički obrađen, te geokemijski podatci dobiveni pomoću rendgenske fluorescencije i masene spektrometrije s induktivno spregnutom plazmom upućuju na to kako su minerali koji nose Sc raspršeni pretežito u boksitnome, bočno izduženome tijelu nastalom trošenjem ishodišnoga (piroksenskoga) diorita. Spektralni je raspon getita kao minerala koji sadržava Sc od 0,43 do 1,03 μm, s glavnim apsorpcijskim značajkama od 2,0 do 2,4 μm. Nadalje, getit je uglavnom koncentriran na gornjemu boksitnom horizontu koji je u vezi sa strukturama boranja. Minerali koji sadržavaju rudu također su rasprostranjeni u jalovini i u još nekim područjima gdje se oplemenjivalo, ali u relativno niskome udjelu. Ovaj je rad nedvojbeno vrijedan jer prezentira praktičnu upotrebu daljinskoga prediktivnog kartiranja prilikom istraživanja mineralnih sirovina.

Ključne riječi:
skandij, getit, Landsat, ALOS PALSAR, kartiranje

Author's contribution

Rosmalia Dita Nugraheni (1) carried out data collection from satellite images and laboratory analyses, conceptualization, processing of the satellite image, and writing the manuscript, including data presentation and interpretation. **Widya Anggraini** (2) performed the grade domaining, the grade plot for geochemical data, and mineral map. **Naily S. Setiawan** (3) re-drew figures from literature. **Cahyaningratri P. Riyandhani** (4) contributed to the manuscript editing and interpretation of results. **Dewi Syavitri** (5) performed the final check for the article manuscript. **Dedi Sunjaya** (6) conducted a field visit, mapping, and data collection. **Agustinus Nopi** (7) performed a field visit and field data validation. **I Gde Sukadana** (8) examined the results and manuscript editing.